Novel Kinematics of an Anthropomorphic Prosthetic Hand Allowing Lateral and Opposite Grasp with a Single Actuator

Côme Butin, Damien Chablat, Yannick Aoustin, David Gouallier

Côme Butin
Nantes Université, École Centrale Nantes,
CNRS, LS2N, UMR 6004,
44000 Nantes, France
& ORTHOPUS
Assistive technology manufacturer
Nantes, FRANCE
email: come.butin@orthopus.com

Damien Chablat[1]
Nantes Université, École Centrale Nantes,
CNRS, LS2N, UMR 6004,
44000 Nantes, France
email: damien.chablat@cnrs.fr

Yannick Aoustin
Nantes Université, École Centrale Nantes,
CNRS, LS2N, UMR 6004,
44000 Nantes, France
email: yannick.aoustin@univ-nantes.fr

David Gouaillier
ORTHOPUS,
Assistive technology manufacturer
Nantes, FRANCE
email: david.gouaillier@orthopus.com

Novel Kinematics of an Anthropomorphic Prosthetic Hand allowing Lateral and Opposite Grasp with a Single Actuator

This work introduced a new hand prosthesis architecture able to achieve an opposite and lateral grasp by using a single actuator. An analysis of the hand prostheses, as well as the movements classically performed in daily life and at work allows us to focus our work on these two types of grasp. A lockable passive joint is moved by the user to switch between the opposite and lateral grasp. The location of the thumb was defined thanks to 3D scans in four extreme positions. The movement of the thumb is analysed to determine the location of the joints to be created. Then, a four-bar linkage was optimized to realize this motion with good force transmission. A sensitivity analysis was performed to evaluate the performance index variation based on design parameters.

Keywords: Hand prosthesis, thumb position, motion transmission, lateral and opposite grasp.

1 Introduction

Providing helpful hand prostheses to users in need is a very challenging task. Since the 1970s, various myoelectric prostheses have been developed. The first prostheses were designed with only one degree of actuation (DoA) to be simple and robust. The only grasping mode was the opposite pinch also called tridigital grasp. Some tridigital prostheses are still sold such as the VariPlus Speed (Ottobock[2]) and even new ones are launched on the market such as the Myo Kinisi (Steeper[3]) in 2021. More advanced prostheses are currently available on the market such as the i-Limb (Össur / Touch Bionics[4]), the Bebionic hand (Ottobock), or more recently the TASKA hand (TASKA Prothetics[5]) and the COVVI hand (COVVI[6]). These prostheses have articulated phalanxes on each finger, and are equipped with up to six actuators to drive 10 to 11 joints. They are able of achieving a large number of grip patterns to provide more functionality to the user. While much effort is invested in designing new multi-grip pattern prostheses[7], these prostheses are often known for their lack of mechanical robustness, their poor speed and force performances [1], their control complexity, their heavy weight, and their very high price.

Hand prostheses with intermediate technical choices have been developed to limit the number of motors needed while providing more functionality and esthetics than tridigital prostheses. Indeed, restraining the number of actuators seems to be a reasonable choice to develop an accessible prosthetic hand (affordable, easy-to-use, robust, and easy-to-repair). This allows us to decrease the complexity of the hand, thus reducing its price and the weight of the battery, increasing the robustness of the hand and intuitive user control.

The Michelangelo hand (Ottobock) uses two actuators. A large flat brushless motor is used to transmit the flexion movements to the upper fingers and to the thumb, while the abduction of the thumb is realized by a second small motor integrated into the thumb body [2]. The Michelangelo offers two grasps to the user: the opposite grasp and the lateral grasp. Another mechanism has been patented [3] by the start-up BionIT Labs and is probably used in their Adam's Hand. This mechanism uses a single motor to actuate the whole hand with a set of geared differentials to distribute the force to all the fingers. Such a device requires tiny gears, and necessitates to be precisely machined and assembled, leading to high financial costs, and a lack of robustness. The Hannes hand [4], not yet available on the market, is also motorized with a single DC motor. Its sub-actuation mechanism is based on thin cables routed inside the hand through a large number of pulleys. This also seems difficult to provide robustness with good speed and force performances with this architecture.

Different academic works proposed sub-actuation mechanisms to drive all fingers with a single actuator. Some studies are focusing on tendon-based differential mechanism [5–7] to distribute the forces to each finger using cables. Other works generate a linear movement along the abduction axis of the thumb [8, 9]. The linear moving shaft is attached to the thumb through a mechanical linkage to transmit the flexion movement. This mechanism is working both in lateral grasp and opposite grasp while the linear driving shaft can rotate on itself and continue to transmit the movement. The upper fingers are driven through a tendon-based differential. [10] developed a comparable solution where a screw-nut transmission is placed along the thumb abduction axis. The screw is driven by the motor, and the nut is driving the thumb using a linkage. In these three works, the abduction axis is placed vertically in the palm to get the place to integrate all components. This placement is not the best option for anthropomorphism. This mechanism also needs to generate a linear movement from a rotationnal motor, which can be difficult if force and speed are needed in the whole range of mo-

[1] Corresponding Author.
April 3, 2023
[2] https://www.ottobock.fr
[3] https://www.steepergroup.com
[4] https://www.ossur.com
[5] https://www.taskaprosthetics.com
[6] https://www.covvi.com
[7] https://bionicsforeveryone.com/worldwide-explosion-in-bionic-hand-technology\-continues/

tion. Finally, [11] is using a planar linkage to realize two different opposite grips, which does not permit thumb abduction.

Ottobock also patented a new design of a Michelangelo-like prosthesis using a single motor instead of two [12]. In this version, an eccentric pin is driven by the flat motor with its axis mounted normally to the palm. The eccentric is mounted by a mechanical coupler to the thumb through universal joints. From an open position where the eccentric is at the lowest distance of the thumb base, the eccentric can move in one direction to close the thumb in the opposite grasp or move in the other direction to close the thumb in a lateral grasp. This version could be adapted for a smaller version of Michelangelo hand, but has not been commercialized.

In each of the previously presented prosthesis except the Michelangelo, the fingers are composed of two or three coupled phalanxes that move together, to mimic the human hand behavior. This finger design allows grasping different shapes of objects while keeping a large number of contact points to ensure proper grasping stability. However, by measuring the performances of able-bodied subjects using SHAP test while blocking different degrees of freedom (DoF), Montagnani showed that rigid upper fingers can be sufficient to provide good grasping capabilities [13, 14].

To answer the problems of accessibility and simplicity, our selected strategy is to develop a new prosthesis with a single actuator, which can realize lateral grasp and opposite grasp. In the proposed version, the change between grasping modes is done by rotating manually the thumb on an abduction axis. The index and the middle fingers are moving as one solid, while the ring finger and the little finger are cosmetic and are not transmitting efforts. This prosthesis should close its finger in less than 0.5 seconds and apply a force at fingertips greater than 70 N both in lateral grasp and opposite grasp. This work was conducted in collaboration with the BionicoHand project [8], which aims to develop an accessible, robust, and powerful Open Source prosthesis.

In the first attempt of developing such a prosthesis [15], we encountered the difficulty of constructing new kinematics with the anthropomorphic results, which can be a source of rejection for users. In this study, we developed a new method to construct the kinematic architecture of our hand from the 3D scan of a hand, to be the more anthropomorphic possible. We also tried to transmit the flexion movement of the upper fingers to the thumb with cables to facilitate design and integration, but cables show their limits when transmitting high efforts. Here, we propose a rigid transmission based on a rod linked to the upper fingers and to the thumb with ball joints. While four-bar linkage is widely used and optimized [16] for the sub-actuation of prosthetic fingers, no other hand prototype using rigid linkage to transmit movement between upper fingers and thumb has been found in the literature. This new mechanism has several design parameters which have to be refined to realize the two different grasping modes. An optimization process and the validation criteria are studied here. This design process precisely detailed here is also a major contribution that enables the understanding of this mechanism and its adaptations in the next iterations of hand prosthesis, with new inputs or slightly different design constraints.

This paper is outlined as follows. Firstly, we review the different available kinematic architecture in available prostheses, in order to propose a new kinematic architecture in Section 2. Then, we propose a method to construct an anthropomorphic hand with one DoF upper fingers and two DoF thumb in Section 3. In Section 4, we propose a new type of transmission using a rod and the optimization process to size such a system according to different design constraints. Finally, Section 5 presents the conclusions and several directions for future work.

2 Kinematic architecture choice

While adding degrees of freedom and more actuators to myoelectric hands increases the number of achievable grasps, it also increases the complexity and price of the prosthesis, thus reducing its accessibility. We try here to compare the benefits of different kinematics, giving the ability to select a kinematic architecture that is a trade-off between grasping capabilities and simplicity.

2.1 Manipulation taxonomy and frequency of use. It is important to be able to evaluate the value of the choices made on existing prostheses to decide on a relevant architecture. The use of a grasp taxonomy is helpful. Here we choose Bullock's taxonomy [17] shown in Fig. 1, which provides frequencies of use for each grasp during workshop and household tasks. This taxonomy excludes voluntarily the non prehensile grasp patterns and the natural rest position of the hand.

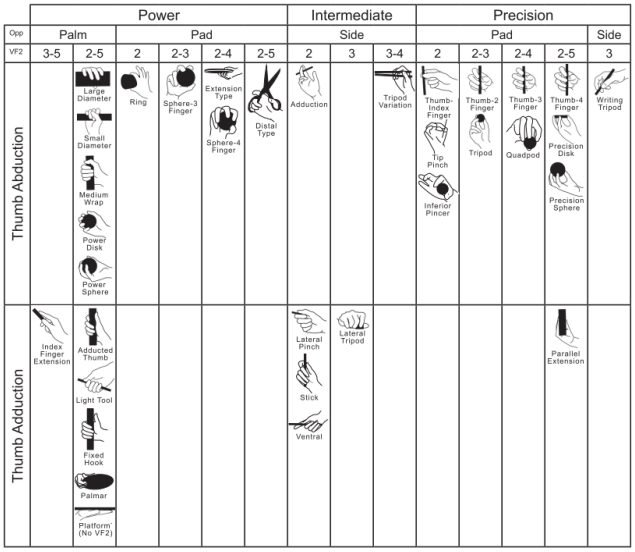

Fig. 1 Taxonomy of object grasp [17]

By observing the frequencies of the ten most used grasps, it has been noticed that seven of then use the thumb in opposition (for a total frequency of 49.7%) while three others use the thumb in lateral position (for a total frequency of 21.3%).

2.2 Kinematic architectures of robotic hands. We selected four different prostheses on the market to represent the different prostheses architecture and evaluate them. The most recent prosthesis (TASKA Hand) is presented on Fig. 2.

2.2.1 VariPlus Speed. This tridigital prosthesis is the last generation of trigital prostheses made by Ottobock providing a single grasping mode. The performances declared by Ottobock are 100 N of grasping force and 300mm/s of closing speed. The upper fingers are driven by the motorization using partial spur gears. The thumb is linked to the thumb palm with a rod to form a four bar linkage. Such transmission is described in [15].

2.2.2 Michelangelo hand. This prosthesis is proposed by Ottobock, and provides two grasping modes: lateral and opposite. To change the grasping mode, the user can use co-contractions or stay contracted after entire opening of the hand. A motor then changes the thumb to lateral position or opposite position. The upper fingers flexion axis is not parallel. Instead, a slight offset permits to spread the fingers when opening the hand, as a natural hand would do. The performances declared by Ottobock are about 60 N to 70 N of grasping force and 300 mm/s of closing speed.

2.2.3 i-Limb hand. The i-Limb has been developed by Touch Bionics as one of the first multi-grip patterns myoelectric hand, and

[8] https://bionico.org/

Fig. 2 Four prostheses available in the market in 2022. Upper left: i-Limb (Össur). Upper right: VariPlus Speed (Ottobock). Lower left: TASKA hand (TASKA Prosthetics). Lower right: Michelangelo hand (Ottobock).

then bought by Össur. This hand is capable of 18 predefined patterns and is available with different options (Access, Quantum, Ultra) such as size, materials, passive thumb abduction or motorized thumb abduction. This prosthesis has vertical thumb abduction mechanism and fully parallel upper fingers, leading to a robotic but not anthropomorphic design. The closing time is announced at 0.8 seconds, with a pinching force measured under 20 N [1] produced by the different motors in each finger body. This hand is appreciated for its finesse but is also known by some users for its fragility and its poor performances.

2.2.4 TASKA hand. This multi-grip patterns hand has been recently developed as first waterproof myoelectric prosthesis, and is focusing on robustness. 23 patterns are predefined and personalized grips can be defined by the user. Each finger and its motor are mounted on a compliant chassis which allows passive lateral abduction of the upper fingers. This compliance is supposed to allow more dexterity on some grip patterns. A trigital pinch is announced at 25 N of force, for about 1 second of closing time (estimated from the given finger speed).

2.3 Selected architecture. Scoring the functionality of the different prostheses, that is, their ability to perform actions and inputs desired by the user would be really helpful to select the best kinematic architecture. Several methods of clinical evaluation can be used to quantify the functionality of a prosthesis, such as the SHAP test [18] or the OPUS test [19]. Nevertheless, these clinical trials are expensive and few prostheses have been evaluated. The coexistence of several tests does not allow easy comparison.

By linking the four described prostheses to the grasp taxonomy, we observe a large gap of grasp reproducibility between the trigital prosthesis that does not enable lateral grasp and the three others. While the greater number of DoF on multi-grasp patterns hands add even more possibilities in term of grasp, the gap of functionality between the Michelangelo and the multi-grasp patterns hands is less important than the gap with trigidital hand. Moreover, the complexity needed with adding a high number of DoF increases the price of the device, its weight, and its energy consumption while lowering robustness, reparability, and control intuitiveness.

In order to propose an accessible prosthetic hand, we choose here to develop a new kinematic architecture that enables both opposite and lateral grasps while limiting the number of DoF. This kinematics provides one joint for each upper finger and two joints at the base of thumb, as presented on Fig. 3. All the upper fingers are moving together, even if the joints are not aligned. The ring and the little fingers are not designed to transmit grasping force, only following the other fingers.

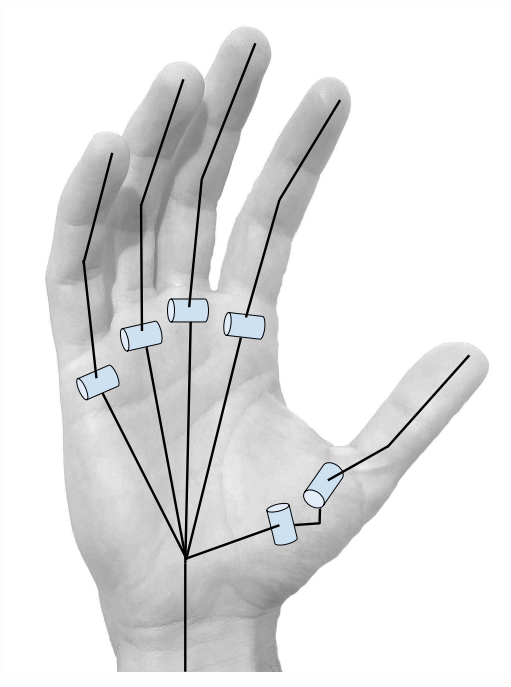

Fig. 3 Selected kinematic architecture. Each upper finger has one degree of freedom (flexion - extension) while the thumb has two degrees of freedom (flexion - extension, palmar abduction - radial abduction).

About thumb kinematics, we would like to be able to completely decouple the abduction movement used to change the grasp on a joint axis, from the flexion movement used to tighten on the other joint axis. Figure 4 shows the desired movements between the different positions of the thumb. The thumb abduction joint can be left passive to reduce the complexity of the device. This joint can be indexable to set manually the thumb either in the opposite or lateral position.

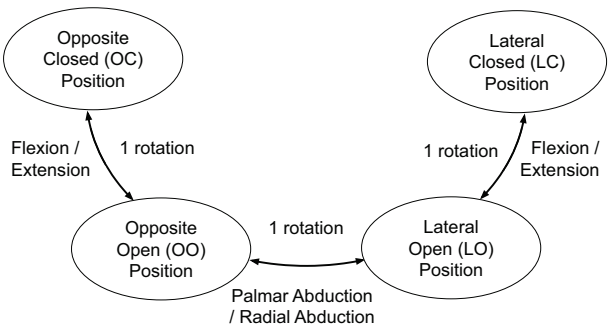

Fig. 4 Diagram showing the four extreme positions of the thumb in the prosthesis and the three movements of rotation

3 Anthropomorphic placement of finger links

The aesthetics of the prosthesis is essential for its acceptance. The placement and movement of the fingers are factors influencing the aesthetics. Some companies choose to assume the robotic aspect of the prosthesis with parallel upper fingers, and a 90° rotation

between the lateral position and the opposite position, as on the i-Limb prosthesis. Others prefer a more anthropomorphic appearance allowing the user to conceal his disability better if he wishes. The placement of the fingers is more "organic" with less aligned fingers and less conventional angles of rotation. This approach has been adopted, since the discretion of the prosthesis can help its acceptance, especially in countries where disability can be a source of discrimination.

3.1 Placement of the thumb flexion and abduction axes. The kinematic construction of the thumb is more complex than that of the upper fingers, since the thumb is linked to the palm by two links in series, and must make it possible to achieve a stable grasp in the opposite grasp as in the lateral grasp.

3.1.1 Screw transformation formalism. In order to describe the revolute joints and the movements of the thumb, we use here screw transformation formalism. Any transformation of space can be expressed as a rotation about an axis Δ and a translation along the same axis. This representation is called a screw.

A transformation from one frame of reference i to another j in its homogeneous form is described by a matrix ${}^{j}\boldsymbol{T}_{i}$ containing the coordinates of frame of reference i expressed with respect to the frame of reference j. This homogeneous matrix is composed of a rotation matrix ${}^{j}\boldsymbol{R}_{i}$ and a translation ${}^{j}\boldsymbol{p}_{i}$ such that

$$ {}^{j}\boldsymbol{T}_{i} = \begin{bmatrix} {}^{j}\boldsymbol{R}_{i} & {}^{j}\boldsymbol{p}_{i} \\ \boldsymbol{0}^{\top} & 1 \end{bmatrix} \tag{1} $$

$$ {}^{j}\boldsymbol{R}_{i} = \begin{bmatrix} r_{11} & r_{12} & r_{13} \\ r_{21} & r_{22} & r_{23} \\ r_{31} & r_{32} & r_{33} \end{bmatrix} \tag{2} $$

$$ {}^{j}\boldsymbol{p}_{i} = \begin{bmatrix} p_x \\ p_y \\ p_z \end{bmatrix} \tag{3} $$

The representation in the form of a screw is defined by a point $\boldsymbol{\rho}$ belonging to the axis of rotation Δ, a unit vector $\hat{\boldsymbol{\omega}}$ along the direction of the axis, an angle of rotation Θ around the axis Δ and a translation h along Δ. The passage from the homogeneous transformation to this representation is given in [20], with $\boldsymbol{l}$ an intermediate calculation vector:

$$ \boldsymbol{l} = \begin{bmatrix} r_{32} - r_{23} \\ r_{13} - r_{31} \\ r_{21} - r_{12} \end{bmatrix}^{\top} \tag{4} $$

$$ \Theta = \operatorname{sign}(\boldsymbol{l}\ {}^{j}\boldsymbol{p}_{i}) \left| \arccos\left(\frac{r_{11} + r_{22} + r_{33} - 1}{2} \right) \right| \tag{5} $$

$$ h = \frac{\boldsymbol{l}\ {}^{j}\boldsymbol{p}_{i}}{2\Theta \sin\Theta} \tag{6} $$

$$ \boldsymbol{\rho} = \frac{(\boldsymbol{I}_{3\times 3} - {}^{j}\boldsymbol{R}_{i}^{\top})\ {}^{j}\boldsymbol{p}_{i}}{2(1 - \cos\Theta)} \tag{7} $$

$$ \hat{\boldsymbol{\omega}} = \frac{\boldsymbol{l}}{2 \sin\Theta} \tag{8} $$

We remark that this representation is using eight parameters (vectors $\boldsymbol{\rho}$ and $\hat{\boldsymbol{\omega}}$, scalars Θ and h), which is superabundant by two. There is one free parameter from $\boldsymbol{\rho}$ that can be fixed arbitrarily and the second superabundant parameter can be found knowing that the norm of $\hat{\boldsymbol{\omega}}$ is equal to 1 [20].

We also remark by this notation that a pure rotation is a screw transformation with $h = 0$, that is to say by retrieving one independent parameter. That way, a pure rotation can be described by five independent parameters or by the seven remaining parameters of screw transformation. The parameter Θ is giving the magnitude of rotation while the six others parameters from $\boldsymbol{\rho}$ and $\boldsymbol{\omega}$, including four independent parameters, are defining the rotation axis.

3.1.2 Problem formulation. Two revolute joints are placed in series to move the thumb. As seen in section 3.1.1, each rotation axis of these joints can be defined by four independent parameters. Eight parameters, therefore, define the placement of these two joints. Three angles of rotation between the four extreme positions of the thumb must be defined, corresponding to the amplitude of movement between the positions as shown in Fig. 4 and bringing to 11 the number of independent parameters to be defined.

In addition to the aesthetic aspect, the movement of the thumb must allow a stable grasp and confidence of the user. Several tests describe the mobility of the thumb. For example, the Kapandji test is used to design of a robotic hand in [21]. These tests are not suitable for such simple kinematics. Instead, observation of natural hand is preferred.

To define the joints of the fingers, we start by defining four extreme positions: closed or open positions for either opposite or lateral grasp. The latter are chosen empirically by observing the natural poses of the hand and the ease of grasp. The four positions are then scanned using a 3D scanner [22]. Figure 5 shows the result of the scan with one gloved hand in the four extreme positions.

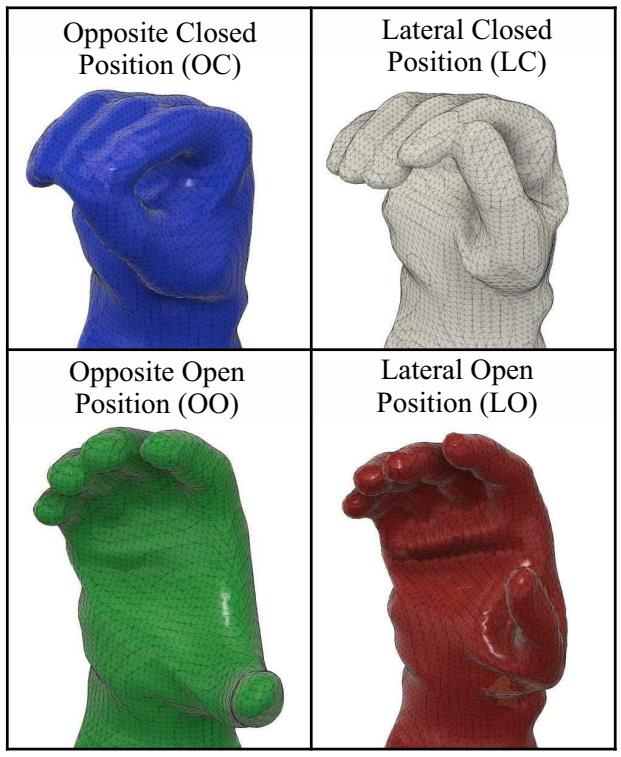

Fig. 5 Scan of the four extreme positions of the thumb

The scanned surfaces are then superimposed so as to have a common landmark. A volume corresponding to the top of the thumb is modeled in the CAD software and is duplicated in different positions to match this volume to the different areas scanned. Figure 6 shows the four superimposed surfaces, with the volume placement of the thumb (in yellow) corresponding to each position.

Four identical volumes are placed in space. By taking a first volume as a reference, this is possible to describe the relative positions and orientations of the three other volumes using three spatial transformations. Each transformation can be described by six in-

Fig. 6 Superposition of the four scanned surfaces and placement of a volume (in yellow) in correspondence of the surfaces

dependent parameters, for a total of 18 independent parameters for the three transformations.

The problem is then to find methods to define the 11 desired geometric parameters (the two rotation axes and the three angles of rotation) from the 18 parameters obtained with the transformations.

3.1.3 Problem simplification. Although it is possible to address this problem in a global way, a direct approach and the use of simple optimization tools have been favored.

Initially, only three positions and two transformations are considered. We choose here not to consider the closed lateral position of the thumb. The problem is then divided into two identical subproblems: define a pivot axis and a rotation angle for each given transformation. It is then a question of defining five geometric parameters from six transformation parameters. The transformation from the opposite closed position to the open opposite position will give the flexion axis, and the transformation from the open opposite position to the lateral open position will give the abduction axis.

In the second step, it is determined whether the resulting axes can be used to place the thumb in an acceptable closed lateral position.

Since this problem is over-constrained, the solution found will depend of chosen resolution approach. The definition of five parameters from six independent parameters will result in information loss, and the resolution approach is to determine which information can be ignored. Two different approaches are evaluated here.

3.1.4 Simplified approach - screw representation. Inherent in the anatomy of the hand, the movement of the thumb corresponds to rotations, without translation. From this observation, the desired axis of rotation movement can be chosen as the one given by the screw representation of the transformation. The translation motion is then ignored, and the rotation angle is given directly by the representation. By ignoring the value of the translation h, we ensure to convert the six independent parameters of a screw transformation to the five independent parameters of a pure rotation transformation.

The resulting rotational motion is slightly different from the initial transformation. Evaluating this shift allows us to assess the suitability of the method for defining the axes of the thumb links. One method to evaluate this shift is to rotate the thumb from the opposite open (OO) position to the other positions

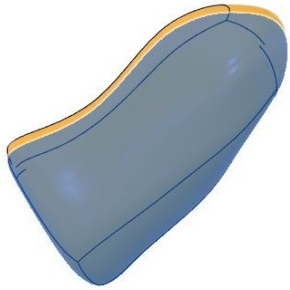

Fig. 7 Superposition of the volume of the thumb in the desired open opposite position (in yellow) and the volume obtained by rotation of the thumb in the opposite closed position (in grey)

$P \in \{OC, LC, LO\}$ according to the constructed axes and then calculate the transformation between the initial marker of the thumb in position P, and the marker obtained by rotation to position P. For example, the thumb is rotated from position OO to position OC, giving a new marker in position OC. The transformation between the initial OC position and the new OC position is computed. Table 1 shows the results of the obtained transformations. The origin of the used frames is placed at the gravity center of the volumes defined during the digitization.

The results obtained are difficult to interpret. If we can easily look at the distance between the centers of gravity of the thumb, defining a relevant measure of a global distance taking into account rotation and position is much more complicated, rotations and translations not being homogeneous.

Another simple solution is to look at the interference between the volume of the thumb obtained by transformation and by pure rotation, as shown in Fig. 7. The interference is measured for each movement, and the results are presented in Table 2.

It is observed that the reconstructed opposite closed and open lateral positions are close to the original positions. The reconstruction of the closed lateral position is less good. This seems to be consistent with the construction method: this position is not included in the calculations to define the axes.

3.1.5 Simplified approach - neutral fiber transformation. The second method of resolution is possible by noticing that the shape of a thumb is close to a cylinder. We can then tolerate a difference in rotation of the thumb around its own axis (or neutral fiber) between the initial transformation and the obtained transformation.

While a translation was ignored in the screw transformation approach, we choose here to ignore a well-chosen rotation.

The neutral fiber of the thumb is represented by a segment **EO** in the two desired positions. It is then a question of finding the unique rotation between the two segments $\mathbf{E}_i\mathbf{O}_i$ and $\mathbf{E}_j\mathbf{O}_j$. Since rotation preserves distances, any point $\mathbf{G}_i$ belonging to the segment $\mathbf{E}_i\mathbf{O}_i$ and its image by rotation $\mathbf{G}_j$ belonging to the segment $\mathbf{E}_j\mathbf{O}_j$ are equidistant from the axis Δ. This axis can be constructed geometrically:

- we construct the segment $\mathbf{E}_i\mathbf{E}_j$, then its mediator plane $\mathcal{P}_\mathrm{E}$;
- we construct the segment $\mathbf{O}_i\mathbf{O}_j$, then its mediator plane $\mathcal{P}_\mathrm{O}$;
- the axis Δ is given by the intersection of the planes $\mathcal{P}_\mathrm{E}$ and $\mathcal{P}_\mathrm{O}$.

The elements of the construction are presented in Fig. 8. As for the previous method, the offset between the transformation and the obtained rotation is evaluated and the results are presented in Table 3.

We observe that the results obtained with this method are better: the interference error is divided by more than three in the closed

Measuring elements	${}^{j}\boldsymbol{R}_{i}$	${}^{j}\boldsymbol{p}_{i}$ [mm]
Transformation between the original OC position (j) and the OC position obtained by flexion rotation (i).	$\begin{bmatrix} 0.985 & 0.037 & -0.170 \\ -0.087 & 0.950 & -0.299 \\ 0.150 & 0.310 & 0.939 \end{bmatrix}$	$\begin{bmatrix} 0.8 \\ -0.1 \\ -1.4 \end{bmatrix}$
Transformation between the original LO position (j) and the LO position obtained by abduction rotation (i).	$\begin{bmatrix} 1.000 & -0.004 & 0.006 \\ 0.004 & 1.000 & 0.005 \\ -0.006 & -0.005 & 1.000 \end{bmatrix}$	$\begin{bmatrix} 1.7 \\ -1.0 \\ -0.2 \end{bmatrix}$
Transformation between the original LF position (j) and the LF position obtained by abduction rotation and then by flexion rotation (i) until index contact.	$\begin{bmatrix} 0.993 & 0.102 & 0.052 \\ -0.108 & 0.984 & 0.142 \\ -0.037 & -0.147 & 0.988 \end{bmatrix}$	$\begin{bmatrix} 7.5 \\ -0.7 \\ -11.0 \end{bmatrix}$

Table 1 Evaluation of thumb axis placement errors by the transformation between the original position and the rotationally reconstructed position expressed in the world frame

Measuring elements	Interference volume	Interference percentage
Initial volume	24.234 cm^3	
Interference in closed opposite position	22.248 cm^3	91.8%
Interference in open lateral position	21.472 cm^3	88.6%
Interference in closed lateral position	9.295 cm^3	38.4%

Table 2 Measurement of the interference rates obtained using the screw representation

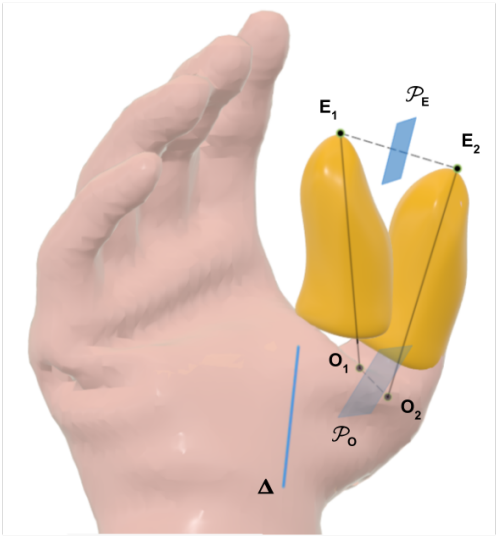

Fig. 8 Definition of the rotation axis Δ by transformation of the neutral fiber

Measuring elements	Interference volume	Interference percentage
Initial volume	24.234 cm^3	
Interference in closed opposite position	23.521 cm^3	97.1%
Interference in open lateral position	23.656 cm^3	97.6%
Interference in closed lateral position	10.722 cm^3	44.2%

Table 3 Measurement of interference rates obtained using the neutral fiber transformation

opposite and open lateral positions. The result is slightly better in the open lateral position but remains far from the original desired position.

3.1.6 Limitations of the method and problem reformulation. The results given by the two previous methods are satisfactory in their precision to obtain three of the four defined positions but do not allow reaching the fourth with precision. The closed lateral positions obtained by the two methods are not considered acceptable according to aesthetic and grasping qualitative criteria.

It is also observed that the axes obtained with both methods are highly dependent on the input data. In particular, the four original thumb poses are fixed by manual registration with the scans, leading to a large variation in the input parameters of the problem. This variation strongly impacts the placement of the two axes. It is also important to put into perspective the need for accuracy with respect to the original positions defined during the scan in an empirical way.

We can then rephrase the requirements of the problem: it is a question of finding a flexion axis and an abduction axis that allow us to obtain four extreme functional positions. The opposite and lateral closed positions must come into precise contact.

In anticipation of the transmission problems, and considering a mechanism close to the one developed in Sec. 2, it is also desired that the flexion angle to move from the open to the closed lateral position be equal to or slightly less than the flexion angle required to move from the open to the closed lateral position. In this case, ten geometrical parameters must be defined.

3.1.7 Empirical resolution of the reformulated problem. The previous results are not satisfactory enough, and more work is needed to set the parameters properly. However, the first methods employed result in a set of initial parameters that are much closer to a viable solution than if they were chosen randomly from a range. In particular, it can be seen that all the rotation axes constructed by the two methods intersect or are close to intersecting around the same point in space, and this point is very insensitive to variations in the input parameters. A sphere of diameter 5 mm is then constructed by observation and all the axes obtained intersect.

By choosing to fix the centre of this sphere as the mandatory point of the passage of the flexion and abduction axes, the number of parameters is reduced. For each pivot link, two parameters are fixed, leaving two parameters per axis to define their direction as well as the angular travels in flexion and abduction, *i.e.* six parameters.

These six parameters can be fixed by trial and error. The thumb is then constructed in the opposite closed position, so as to ensure precision contact between the thumb, index, and middle fingers.

The final construction of the hand is described in Sec. 4 with associated parameterization.

3.2 Placement of the upper fingers axes. Methods have been developed to place the fingers with anthropomorphic results [23]. It uses a simple construction figure to define angles between fingers. We also remark that the fingers are supposed to be spread in the open position, and coming in contact together when closing. This property permits in a prosthetic hand to block very thin objects between the index and middle finger in the closed position, such as credit cards. In this study, placement rules have been first used, and then refined to approximately match the previously shown 3D scans.

4 Transmission of the flexion movement

4.1 Transmission mechanism selection. Once the location of the links has been determined, a solution must be found to transmit the movement from the motorization to the upper fingers and the thumb. We remind that only the thumb flexion is motorized, and the abduction is kept passive and indexable. Thus, the user has to use its opposite hand to change the thumb grasp, or use its environment as an obstacle to push the thumb on one side or the other.

A natural solution to transmit movement to several fingers is to use tendons. These cables are thin and can be routed in different manners to respect the hand anthropomorphism. They are also well adapted to use differential mechanism. Several academic works [6, 7] used such tendons to create a single actuator robot hand. However, there are a lot of limitations. In particular, the cable diameter required to transmit the forces conflicts with the cable diameter allowing small bending radii for good integration. Failure to meet this minimum bending radius would result in a reduction in the life of the cables. The use of textile cables like Dyneema can help to overcome this limitation, but other problems emerge like rope elasticity or end attachment. To the author's knowledge, the True Limb (Unlimited Tomorrow [9]) and the Hero Arm (Open Bionics [10]), both 3D printed prostheses, are the only commercialized prostheses with cables in their transmission.

To overcome the problems of cable transmissions, a transmission using rigid parts is used. This transmission is inspired by the planar four-bar linkage used in tridigital prostheses. The movement of the motorization is transmitted to the upper fingers, although associated technical solutions are not in the scope of this study. The planar four-bar linkage cannot be used in such way. In order to transmit the flexion movement to the thumb while leaving the abduction movement free, it is necessary to add degrees of freedom. A spatial linkage connected to the upper finger and the thumb via two spherical joints is thus chosen. Here, the middle finger and index finger are not sharing the same rotation axis, and we need to choose on which finger the joint will be attached. Preliminary design tests of this mechanism show that the design objectives are more easily respected when the joint is attached to the middle finger. It should be noted that a rod mounted on two spherical joints has a degree of internal mobility along its own axis, which can be eliminated by using a universal joint at one of the two ends. To simplify the understanding of the mechanism, the two spherical joints are retained in the analysis.

Figure 9 depicts the hand and its rod mechanism in two different positions, with the representation of motorized flexion movement of the middle finger and the thumb, and the passive indexable abduction of the thumb.

4.2 Synthesis of a spatial linkage with a rod with two spherical joints.

4.2.1 Parameterization of the mechanism. Here several parameters are listed to ensure a good grasp. Figure 10 shows the placement of the different key points of the mechanism. Points **A** and **B**

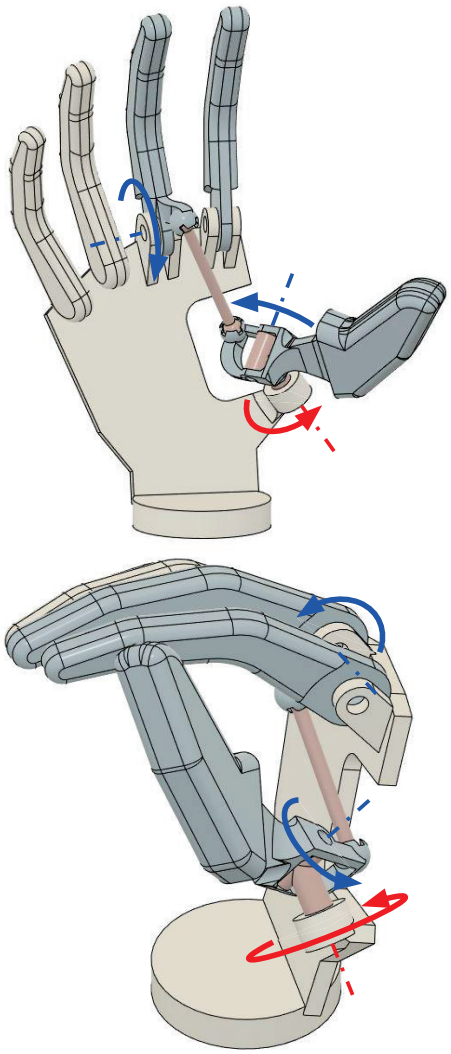

Fig. 9 Principle of transmission of the flexion movement by integrating a rod with two spherical joints between the middle finger and the thumb, with motorized flexion movement in blue and passive abduction movement in red

are the joint centers of the middle finger and the thumb respectively, and have been fixed in Sec. 3. Points **D** and **C** are respectively the centers of each of the two spherical joints. Points **T**, **M**, and **I** are the points where contact with the grasped object is assumed, respectively on the thumb, on the middle finger (for opposite grasp only), and on the index finger (for lateral grasp only).

Figure 11 shows the definition of the rotation axes. The thumb abduction is made around the axis $\overrightarrow{z_t}$ about an angle β. The thumb flexion is realized around the axis $\overrightarrow{u'_t}$ about an angle ϕ. The middle finger rotates around the axis $\overrightarrow{u'_m}$ about an angle θ. In opposite closed position, β=0°, θ=0°, and ϕ is obtained by the kinematic model. $\overrightarrow{v'_m}$ and $\overrightarrow{v''_t}$ are oriented such that they point to the corresponding contacting point, Thus

$$\overrightarrow{v'_m} = \frac{\overrightarrow{AM}}{\left\|\overrightarrow{AM}\right\|}, \quad \overrightarrow{v''_t} = \frac{\overrightarrow{BT}}{\left\|\overrightarrow{BT}\right\|} \tag{9}$$

Table 4 summarizes the coordinates defined in Sec. 3.

[9] https://www.unlimitedtomorrow.com/
[10] https://openbionics.com/en/hero-arm/

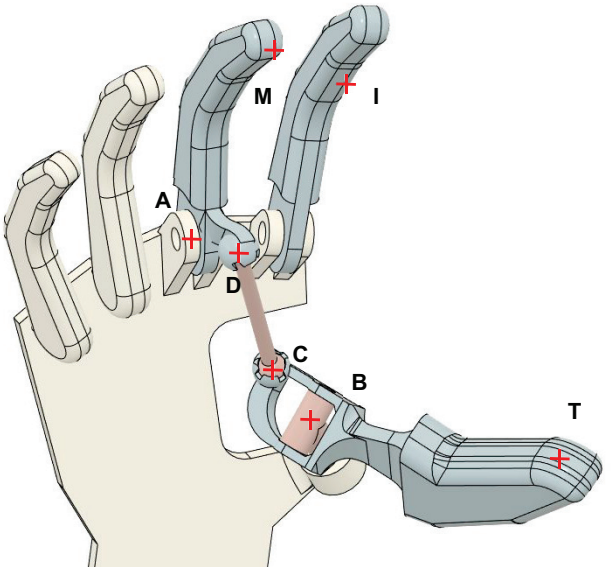

Fig. 10 Placement of the defined points in the mechanism

Points and axes	Values
A	[-25.4, -10.7, 94.8] mm
B	[-8.4, 23.5, 50.6] mm
T	[57.0, 9.5, 115.7] mm
M	[58.2, 3.8, 113.3] mm
I	[34.0, 17.8, 132.6] mm
$\overrightarrow{u_m}$	[-0.13, 0.98, 0.14]
$\overrightarrow{u_t}$	[0.31, -0.42, -0.85]
$\overrightarrow{z_t}$	[-0.25, -0.57, 0.78]

Table 4 The coordinates of the points and axes defining the fingers placement in the opposite closed position, relative to the wrist center, used in Figs. 10 and 11

The positions of the spherical joints of the middle finger (index m) and the thumb (index t) are described in cylindrical coordinates by three parameters and also presented in Fig. 11. The radius r defines the distance between the centre of the spherical joint and the axis of rotation of the finger. The angle α is defined as the angle around the rotation axis between the point of contact of the finger and the center of the joint. The height h corresponds to the position offset along the axis. Finally, the length of the rod is noted l. These parameters facilitate the interpretation of the result since the radius r corresponds to a lever arm for the transmission of the torques.

4.2.2 Synthesis problem formulation. The sizing of this mechanism is important in order to respect the predefined extreme positions and to allow good transmission of forces.

The problem is then to find the parameter vector $\mathbf{P} = [l, \alpha_t, r_t, h_t, \alpha_m, r_m, h_m]$ that allows the thumb to be placed in the four positions defined above.

When the thumb is placed in the opposite grasp, the maximum open position of the middle finger should place the thumb in the open opposite position, and the maximum closed position of the middle finger should place the thumb in the opposite closed position. Similarly, in the lateral grasp, the extreme positions of the middle finger and thumb should be matched. To summarize, the problem to be solved is to match as much as possible the thumb positions induced by the mechanism with the thumb positions previously defined as a reference.

This problem is also subject to several constraints:

(1) certain parameters such as the lever arms r are bounded in order to limit the size of the mechanism;
(2) other parameters are bounded to simplify the integration such as the heights h;
(3) respecting the opposite closed position and the lateral closed position is more important than the other positions, to ensure a fine and precise grasp when the fingers make contact;
(4) the force transmitted by the linkage must be limited to facilitate the design of the mechanism, the lever arms r must thus be sufficiently important;
(5) the torque must be transmitted along the stroke without passing through a singularity, with a transmission factor (mechanical advantage) as constant as possible to avoid oversizing the actuator.

A cost function $\mathcal{C}(\mathbf{P})$ is defined to evaluate whether a selected set of parameters results in acceptable thumb positions, that is to say how much the objective is fulfilled. To do this, the error in the thumb flexion angle φ in each of the four defined positions is measured. We then have a cost $\mathcal{C}(\mathbf{P})$ defined as:

$$\begin{aligned}\mathcal{C}(\mathbf{P}) =& \lambda_C \left(\varphi^P(\theta_C, \beta_{opp}) - \varphi^{ref}_{OppC}\right)^2 \\ &+\lambda_O \left(\varphi^P(\theta_O, \beta_{opp}) - \varphi^{ref}_{OppO}\right)^2 \\ &+\lambda_C \left(\varphi^P(\theta_C, \beta_{lat}) - \varphi^{ref}_{LatC}\right)^2 \\ &+\lambda_O \left(\varphi^P(\theta_O, \beta_{lat}) - \varphi^{ref}_{LatO}\right)^2\end{aligned} \tag{10}$$

where $\varphi^P(\theta, \beta)$ gives the flexion angle of the thumb as a function of the flexion angle of the middle finger θ and the abduction angle of the thumb β, for a vector of parameters $\mathbf{P}$. φ^{ref}_i corresponds to the desired reference value of φ in the given position i. Finally, λ_i corresponds to a weight for each position i allowing us to modulate the importance of the reproduction of each position.

The reference values used in the problem are given in Table 5. These values were defined following the placement of the extreme positions described in Sec. 3. λ_C is set arbitrarily at three times the value of λ_O to give more importance to closed positions according to constraint 3.

Constraints 1 and 2 are easily taken into account by bounding input parameters while searching for solutions. Constraints 4 and 5 have to be validated manually by the designer once a parameter set is chosen. After preliminary results, parameter ranges are adjusted to exclude unsuitable solutions without leaving out too many solutions. These ranges are presented in Table 6. The final solution should be validated after being selected.

We can remark that the range of motion of this mechanism, which corresponds to the maximum opening distance, is set by the reference open positions. Thus, checking the sufficient range of motion of grasping large objects should be done in the phase of finger placement, and not in the phase of mechanism synthesis.

4.2.3 Geometrical resolution of the mechanism. From the middle finger flexion angle θ and the thumb abduction angle β, we need to obtain the thumb flexion $\phi(\theta, \beta)$. This is done by using the equation describing the closing loop:

$$\left\| -\overrightarrow{AD} + \overrightarrow{AB} + \overrightarrow{BC} \right\| = l \tag{11}$$

with :

$$\overrightarrow{AD} = {}^0\boldsymbol{R}_m \left(r_m \overrightarrow{v_m} + h_m \overrightarrow{u_m}\right) \tag{12}$$

$$\overrightarrow{BC} = {}^0\boldsymbol{R}_{ta}\, {}^0\boldsymbol{R}_{tf} \left(r_t \overrightarrow{v_t} + h_t \overrightarrow{u_t}\right) \tag{13}$$

where

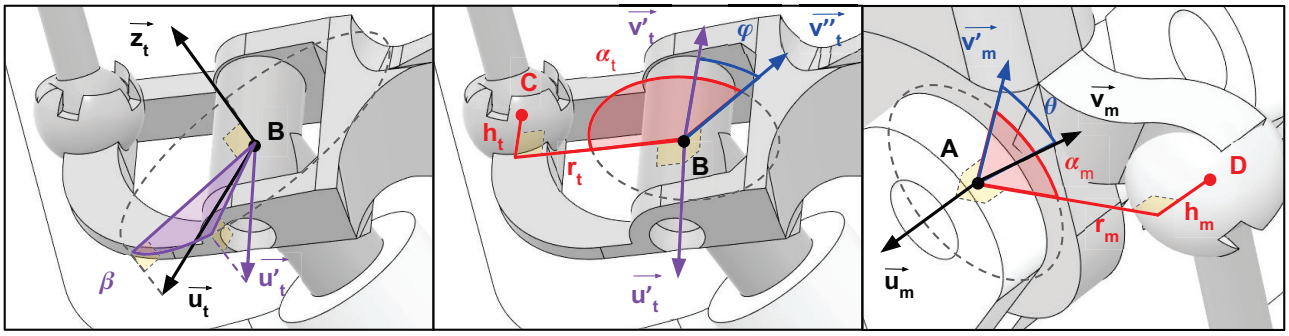

Fig. 11 **Parameters $\mathbf{P} = [l, \alpha_t, r_t, h_t, \alpha_m, r_m, h_m]$ defining the connecting linkage in the prototype**

θ_C	θ_O	β_{Opp}	β_{Lat}	$\varphi^{ref}_{OppC} = \varphi^{ref}_{LatC}$	$\varphi^{ref}_{OppO} = \varphi^{ref}_{LatO}$	λ_C	λ_O
0°	55°	0°	35°	0°	-55°	3	1

Table 5 **Numerical values used to define the cost function (10)**

	l mm	r_m mm	r_t mm	α_m degree	α_t degree	h_m mm	h_t mm
Min	0	12	11	-50°	135°	-5	-7
Max	-	16	16	-20°	190°	0	5

Table 6 **Ranges of parameters l, α_t, r_t, h_t, α_m, r_m, and h_m**

- ${}^0\boldsymbol{R}_m$ is the rotation matrix expressed in the frame 0 that describes a rotation of an angle $(\theta + \alpha_m)$ around the axis $\overrightarrow{u_m}$,
- ${}^0\boldsymbol{R}_{ta}$ is the rotation matrix expressed in the frame 0 that describes a rotation of an angle β around the axis $\overrightarrow{z_t}$,
- ${}^0\boldsymbol{R}_{tf}$ is the rotation matrix expressed in the frame 0 that describes a rotation of an angle $(\varphi + \alpha_t)$ around the axis $\overrightarrow{u_t}$.

4.2.4 Evaluation of the cost function (10) over the ranges of interest. A lot of methods exist to solve minimization problems by converging to solutions, such as gradient descent algorithms, genetic algorithms, or sequential quadratic programming algorithms [24]. These algorithms have different strengths depending on the given problem and the number of parameters to optimize.

In this problem, only seven parameters need to be optimized. Moreover, by the nature of the mechanism, one can very quickly define a bounded interval for each parameter where the solutions can be optimal and physically consistent. However, the problem may have several local minima and this makes it more difficult to find a global minimum.

The problem is then treated in the first step by exploring the workspace of the parameters. Each parameter is sampled in an interval. The sampling is coarse at first, then refined in a second step around the points of interest. This method requires the cost evaluation function (10) must be called N times, N being the product of the number of samples for each parameter. Post-processing and interpretation of the data are straightforward since we have an image of the cost function over an interval. The development time of the algorithm and its validation is also greatly simplified compared to other methods.

The values selected during sampling are presented in Table 7. These parameters were selected after several tests, eliminating the ranges leading to irrelevant results. The angles α are sampled every five degrees, and the lengths l, r, and h are sampled every millimeter, for a total of 275 000 samples.

We first study the subset of the tested $\mathbf{P}$ vectors such that $\mathcal{C}(\mathbf{P}) < \mathbf{50}$ (187 elements / 275 000 tested). This subset permits to better understand what are the best solutions we can obtain. We first remark that the corresponding vectors $\mathbf{P}$ are distributed

Parameters	Sampled values
l	{46, 47, 48, 49, 50, 51, 52, 53, 54, 55, 56} mm
r_m	{12, 13, 14, 15, 16} mm
r_t	{12, 13, 14, 15, 16} mm
α_m	{-50, -45, -40, -35, -30}°
α_t	{145, 150, 155, 160, 165, 170, 175, 180}°
h_m	{-4, -3, -2, -1, 0} mm
h_t	{-7, -6, -5, -4, -3} mm

Table 7 **The values of the parameters tested during the solution exploration**

on almost all the parameters space: for each possible value of the parameters, there is a parameter set $\mathbf{P}$ containing it. This means that the designer could have some flexibility on the parameters to facilitate integration if a good but non-optimal solution is selected.

It is also interesting to study the correlations between the different parameters to better understand their couplings. We apply linear least square regression to each parameter pair. Table 8 presents the linear determination coefficient R^2 for each pair of parameters, which measures the deviation of the points from the determined linear law, between 0 (no correlation at all) and 1 (perfect regression).

	l	r_m	r_t	α_m	α_t	h_m	h_t
l	1	0.015	0.034	0.204	**0.767**	0.020	**0.353**
r_m		1	**0.809**	0.006	0.024	0.000	0.010
r_t			1	0.006	0.030	0.008	0.029
α_m				1	0.004	0.066	0.038
α_t					1	0.030	**0.337**
h_m						1	0.023
h_t							1

Table 8 **The linear determination coefficient R^2 obtained for the linear correlation of each pair of parameters**

We observe a strong correlation between r_t and r_m, and between α_t and l. We can also observe a correlation between h_t and α_t, and a correlation between h_t and l. Figure 12 shows the subset projected to the space of correlated parameters, to observe the relations between parameters.

These correlations do not provide the optimum solution to the problem but are useful for understanding mechanical behavior. This confirms an intuitive hypothesis: the radii r act as lever arms, so their values have to be similar to give a similar range of motion on the upper fingers and thumb. Other correlations, such as between h_t and l, were less predictable.

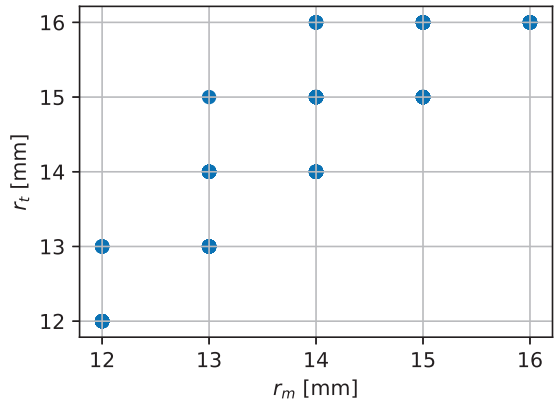

(a)

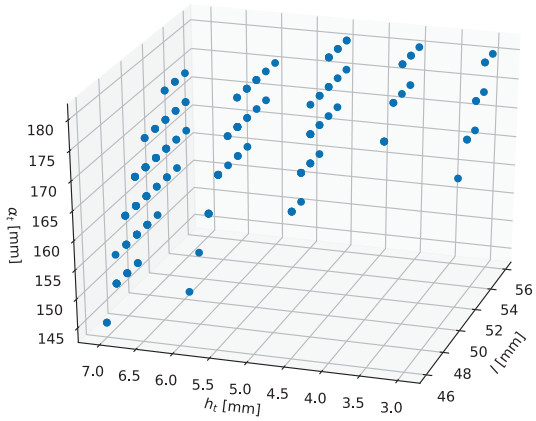

(b)

Fig. 12 Set of parameter vectors P such that $\mathcal{C}(\mathbf{P}) < 50$ with (a) the parameters r_m and r_t, and (b) the parameters l, α_t, and h_t. Reading example: we can find one or more "acceptable" solutions (with $\mathcal{C}(\mathbf{P}) < 50$) where r_m = 14mm and r_t = 15mm while there is no such solution for r_m = 15mm and r_t = 12mm .

4.2.5 Study of local minima and optimization. From the data generated by the exploration of the workspace of the parameters, it is possible to obtain the list of discrete local minima, in the sense of the lowest values among their close neighborhood. We obtain eight discrete local minima, all located at the boundary of the workspace of the studied parameters.

It is interesting to know whether it is possible to optimize the cost function (10) around these minima by considering the continuous parameter space rather than discrete. A solution could be to reduce the sampling steps by a dichotomy to approach the minima sought. This solution is however time-consuming. We are then interested in minimization algorithms for continuous multi-variable functions.

We use here a successive quadratic optimization algorithm (Sequential Least SQuares Programming - SLSQP) to find the local minima closest to an initial value. This algorithm allows to minimize a non-linear cost function, taking into account bounds for each parameter. The cost function (10) to be minimized is not necessarily convex on the study interval, and the method used does not guarantee to converge to a local minimum. However, it can converge to a more optimal solution than those obtained by sampling, and it is therefore interesting to use it.

The optimization algorithm is run with different initial values. Particularly, the discrete local minimums are used to initialize the optimization. From these eight initial values, the algorithm is converging six times to a first parameter set with a cost of 34.51, and two times to a second parameter set with a cost (10) of 34.41.

4.3 Theoretical validation of the selected solutions. The two optimal solutions found need to be validated to select the most appropriate one. The validation process has been conducted on the two solutions. Thus, only the results of the first solution are shown here, which appears to minimize the effort in the connecting rod.

The selected optimal parameter is defined by the following values :

$$\mathbf{P_{opt}} = [48, 16, 16, -50, 155.5, 0, -7] \tag{14}$$

4.3.1 Efforts computation. In order to validate the selected solution, it is necessary to study the grasping force F_{grasp} generated by an input torque τ_{in} exerted by motorization on upper fingers. This force can be calculated by expressing the static equilibrium of torques on flexion axes of upper fingers and thumb, with F_{rod} the force transmitted by the rod. No friction is considered during grasping, and the grasping force direction is defined by the unit vector $\overrightarrow{MT}/\left\|\overrightarrow{MT}\right\|$ between the contacting point of the thumb **T** and the contacting points of the upper fingers **M** as shown on Figure 10. The corresponding equations are given in Eq. (15) for the opposite grasp.

$$\begin{bmatrix} (\overrightarrow{AM} \times \frac{\overrightarrow{MT}}{\left\|\overrightarrow{MT}\right\|}) \cdot \overrightarrow{u_m} & (\overrightarrow{AD} \times \frac{\overrightarrow{DC}}{\left\|\overrightarrow{DC}\right\|}) \cdot \overrightarrow{u_m} \\ (\overrightarrow{BT} \times \frac{\overrightarrow{MT}}{\left\|\overrightarrow{MT}\right\|}) \cdot \overrightarrow{u_t'} & (\overrightarrow{BC} \times \frac{\overrightarrow{DC}}{\left\|\overrightarrow{DC}\right\|}) \cdot \overrightarrow{u_t'} \end{bmatrix} \begin{bmatrix} F_{\text{grasp}} \\ F_{\text{rod}} \end{bmatrix} = \begin{bmatrix} \tau_{in} \\ 0 \end{bmatrix} \tag{15}$$

For the lateral grasp, the grasping force direction is then defined by the unit vector $\overrightarrow{IT}/\left\|\overrightarrow{IT}\right\|$, and the corresponding equations are given in Eq. (16).

$$\begin{bmatrix} (\overrightarrow{AI} \times \frac{\overrightarrow{IT}}{\left\|\overrightarrow{IT}\right\|}) \cdot \overrightarrow{u_m} & (\overrightarrow{AD} \times \frac{\overrightarrow{DC}}{\left\|\overrightarrow{DC}\right\|}) \cdot \overrightarrow{u_m} \\ (\overrightarrow{BT} \times \frac{\overrightarrow{IT}}{\left\|\overrightarrow{IT}\right\|}) \cdot \overrightarrow{u_t'} & (\overrightarrow{BC} \times \frac{\overrightarrow{DC}}{\left\|\overrightarrow{DC}\right\|}) \cdot \overrightarrow{u_t'} \end{bmatrix} \begin{bmatrix} F_{\text{grasp}} \\ F_{\text{rod}} \end{bmatrix} = \begin{bmatrix} \tau_{in} \\ 0 \end{bmatrix} \tag{16}$$

The study of this transmission factor allows first of all to ensure the absence of singularity along the finger stroke. Indeed, a singularity results in a transmission factor that tends to infinity. Secondly, the consistency of the transmission factor allows the motor to be sized precisely and controlled more easily by the user. The result of the grasping force computation with an input torque τ_{in} = 10 N.m is shown in Fig. 13. We remark that all the efforts in the mechanism are proportional to the input torque and the given results are scalable for future motorization sizing. Here we see a variation of 25% of its maximum force along the stroke in the opposite grasp as in the lateral grasp. This variation is equivalent to the force variation in tridigital prostheses [15] and is considered acceptable.

It is also important to see the force transmitted by the connecting rod. This should not be too high in order to allow the correct dimensioning of the connecting rod and the ball joints. Corresponding graphs are shown in Fig. 14.

Finally, the reaction torque in the thumb along the abduction axis is estimated from the previously calculated forces F_{grasp} and F_{rod} using Eqs. (17) and (18) in opposite grasping and lateral grasping respectively. This must be lower than the torque required for manual indexing of the thumb, otherwise, the thumb would change position during tightening. The results are shown in Figure 15.

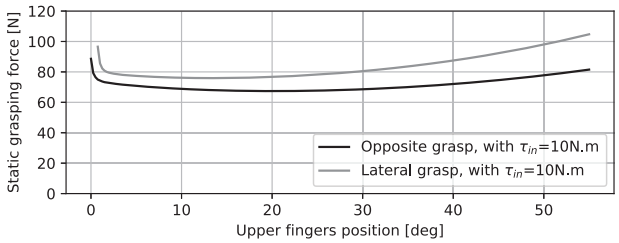

Fig. 13 Grasping force F_{grasp} at the fingertips depending on the position of the upper fingers θ for the optimal parameter set

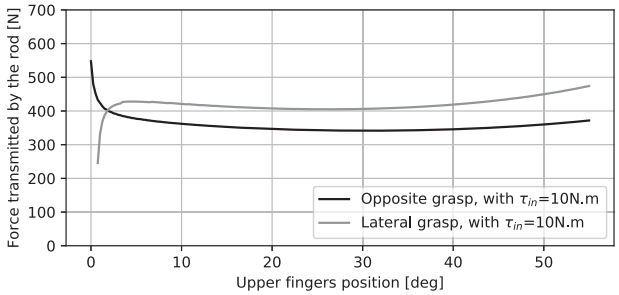

Fig. 14 The resulting force F_{rod} in the connecting rod depending on the position of the upper fingers θ for the optimal parameter set

$$\tau_{abd} = F_{\text{grasp}}(\overrightarrow{BT} \times \frac{\overrightarrow{MT}}{\left\|\overrightarrow{MT}\right\|}) \cdot \overrightarrow{z_t} + F_{\text{rod}}(\overrightarrow{BC} \times \frac{\overrightarrow{DC}}{\left\|\overrightarrow{DC}\right\|}) \cdot \overrightarrow{z_t} \quad (17)$$

$$\tau_{abd} = F_{\text{grasp}}(\overrightarrow{BT} \times \frac{\overrightarrow{IT}}{\left\|\overrightarrow{IT}\right\|}) \cdot \overrightarrow{z_t} + F_{\text{rod}}(\overrightarrow{BC} \times \frac{\overrightarrow{DC}}{\left\|\overrightarrow{DC}\right\|}) \cdot \overrightarrow{z_t} \quad (18)$$

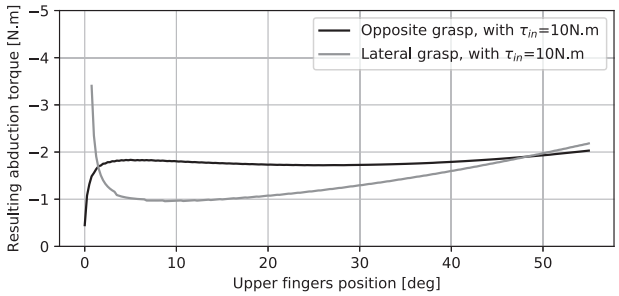

Fig. 15 The resulting torque τ_{abd} on the thumb along its abduction axis depending on the position of the upper fingers θ for the optimal parameter set

We remark large variations of the efforts near the closed positions. It can be explained by the choice of contacting points, which are considered constant, and does not vary during the grasp. Thus, the direction of the grasping force does not reflect reality. Further analysis could help to refine the forces for very low opening angles.

4.3.2 Solution sensitivity evaluation. Finally, the sensitivity of the mechanism to the variation of the parameters is studied. We estimate for each parameter a variation due to the manufacturing and the assembly: $\delta = 0.1$mm for the lengths and $\delta = 0.5°$ for the angles.

Firstly, we measure independently the influence of each parameter p_i, with the integer $i = 1...7$. Figure 16 shows the cost function (10) of the variation between -2δ and 2δ of each parameter. The most sensitive parameters can be easily observed: the length of the connecting rod l and the angles α increase the score obtained by about 10 % for a variation of 1 δ.

We also estimate the combined variation of several parameters by computing the cost function (10) associated with each possible set of parameters $\mathbf{P}$, where the parameters p_i are included in the set $p_i - \delta, p_i, p_i + \delta$. The maximum score obtained is then 47.9, which is 40% higher than the initial score. This variation is important and shows that this is necessary to keep tolerances and clearances during the design as low as possible, especially for the angles and the rod length, while keeping in mind that too tight tolerances will increase the manufacturing cost.

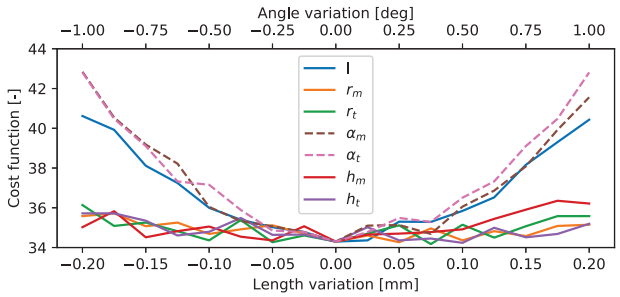

Fig. 16 Sensitivity analysis of the cost function (10) according to the variation of each parameter

4.4 Experimental geometric validation of the selected solutions. In order to validate the design process, we developed a 3D printed model as shown in Fig. 17. Although this manufacturing method lacks of precision, the prototype is able to achieve the four extreme positions and the movements between these positions. The model permits to validate the geometrical analysis and optimization of the mechanism.

5 Conclusions and future work

This paper presents a new prosthesis architecture, with an anthropomorphic aestheticism, and an optimized rigid transmission that permits to achieve both an opposite and lateral grasp. Methods for obtaining the hand kinematics are detailed, and the resulting kinematics are analyzed. The aim of this project is to create a new accessible myoelectric hand, combining good performance, anthropomorphism, and simple mechanical design.

The mechanism has been analyzed to validate the concept. The transmitted efforts show that the performances are sufficiently constant in the range of motion, and sensitivity analysis gives manufacturing tolerances to reach according to specifications. The resulting prosthetic hand could attain tridigital prosthesis performances and robustness while giving more functionalities and aestheticism to users' daily life at a reasonable financial cost.

The design process proposed in this work enables the understanding of this mechanism, using for example correlation analysis. It also enables running the optimization and validation process with new thumb positions as inputs or different design constraints if grasping measurements or user feedback highlights such needs.

While a sensitivity analysis to design parameters has been conducted, this study does not evaluate the impact of input geometry

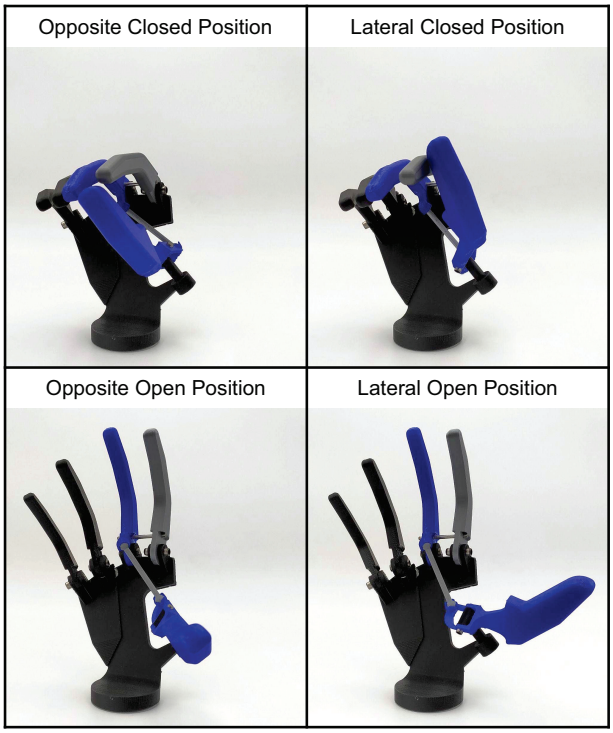

Fig. 17 3D printed model of the proposed mechanism as a proof of concept, in the four extreme positions

variation. Such evaluation would be interesting to validate the robustness of design against manufacturing inaccuracies.

A first experimental validation has been proposed in this paper, that validates the feasibility of such a presented mechanism and the geometrical analysis that has been conducted.

About perspectives, we plan to develop an entirely functional prototype on which we could validate the force analysis developed here. The development and the mechanical integration of such a prototype could also help to highlight the principal drawbacks of the linkage. For this, more work on motorization is necessary. Indeed, obtaining the desired torque and speed with a small and lightweight motor and with an energy consumption problem is not an easy task. The design of a load adaptive variable transmission has been investigated in [25], and further work on non-backdrivable mechanisms and motorization will be conducted.

A second step would be to evaluate the grasping performance using SHAP test [18] or OPUS test [19], and to confront it to users, with the aim to integrate their feedback in further developments.

Acknowledgment

The authors thank Luc Doppler and Okba Mostefaoui for their preliminary studies during their internship at Orthopus company and Nicolas Huchet for his valuable advice on the use of hand prostheses.

Funding Data

This research was supported by ANRT CIFRE grant n°2019 /1721 which funded the first author's doctoral studies.

References

[1] Belter, J. T., Segil, J. L., Dollar, A. M., and Weir, R. F., 2013, "Mechanical design and performance specifications of anthropomorphic prosthetic hands: A review," The Journal of Rehabilitation Research and Development, **50**(5), pp. 599–618.

[2] Puchhammer, G., 2011, "Hand prosthesis with fingers that can be aligned in an articulated manner," US Patent 7,867,287.

[3] Zappatore, G. A., 2020, "Underactuated robotic hand," US Patent App. 16/341,730.

[4] Laffranchi, M., Boccardo, N., Traverso, S., Lombardi, L., Canepa, M., Lince, A., Semprini, M., Saglia, J. A., Naceri, A., Sacchetti, R., Gruppioni, E., and De Michieli, L., 2020, "The Hannes hand prosthesis replicates the key biological properties of the human hand," Science Robotics, **5**(46), p. eabb0467.

[5] Leddy, M. T. and Dollar, A. M., 2018, "Preliminary Design and Evaluation of a Single-Actuator Anthropomorphic Prosthetic Hand with Multiple Distinct Grasp Types," *2018 7th IEEE International Conference on Biomedical Robotics and Biomechatronics (Biorob)*, IEEE, Enschede, pp. 1062–1069, doi: 10.1109/BIOROB.2018.8487198.

[6] Belter, J. T. and Dollar, A. M., 2013, "Novel differential mechanism enabling two DOF from a single actuator: Application to a prosthetic hand," *2013 IEEE 13th International Conference on Rehabilitation Robotics (ICORR)*, IEEE, Seattle, WA USA, pp. 1–6, doi: 10.1109/ICORR.2013.6650441.

[7] Kontoudis, G. P., Liarokapis, M. V., Zisimatos, A. G., Mavrogiannis, C. I., and Kyriakopoulos, K. J., 2015, "Open-source, anthropomorphic, underactuated robot hands with a selectively lockable differential mechanism: Towards affordable prostheses," *2015 IEEE/RSJ International Conference on Intelligent Robots and Systems (IROS)*, IEEE, Hamburg, Germany, pp. 5857–5862, doi: 10.1109/IROS.2015.7354209.

[8] Xu, K., Liu, H., Zenghui Liu, Du, Y., and Zhu, X., 2015, "A single-actuator prosthetic hand using a continuum differential mechanism," *2015 IEEE International Conference on Robotics and Automation (ICRA)*, IEEE, Seattle, WA, USA, pp. 6457–6462, doi: 10.1109/ICRA.2015.7140106.

[9] Liu, H., Bin, Z., Liu, Z., and Xu, K., 2020, "Design of a Lightweight Single-Actuator Multi-Grasp Prosthetic Hand with Force Magnification," Journal of Mechanisms and Robotics, **12**(5), pp. 1–33.

[10] Zheng, Y., Li, X., Tian, L., and Li, G., 2018, "Design of a Low-Cost and Humanoid Myoelectric Prosthetic Hand Driven by a Single Actuator to Realize Basic Hand Functions," *2018 IEEE International Conference on Cyborg and Bionic Systems (CBS)*, IEEE, Shenzhen, pp. 603–606, doi: 10.1109/CBS.2018.8612255.

[11] Wattanasiri, P., Tangpornprasert, P., and Virulsri, C., 2018, "Design of Multi-Grip Patterns Prosthetic Hand with Single Actuator," IEEE Transactions on Neural Systems and Rehabilitation Engineering, **26**(6), pp. 1188–1198.

[12] Eder, F., 2021, "Gripping device," US Patent App. 15/733,337.

[13] Montagnani, F., Controzzi, M., and Cipriani, C., 2015, "Is it Finger or Wrist Dexterity That is Missing in Current Hand Prostheses?" IEEE Transactions on Neural Systems and Rehabilitation Engineering, **23**(4), pp. 600–609.

[14] Montagnani, F., Controzzi, M., and Cipriani, C., 2016, "Independent Long Fingers are not Essential for a Grasping Hand," Scientific Reports, **6**(1), p. 35545.

[15] Butin, C., Chablat, D., Aoustin, Y., and Gouaillier, D., 2022, "Cinématique d'une Prothèse de Main Myoélectrique Accessible avec Actionneur Unique et Rétropulsion Passive du Pouce," *Congrès Français de Mécanique*.

[16] Birglen, L., Laliberté, T., and Gosselin, C., 2008, "Optimal Design of Underactuated Fingers," *Underactuated Robotic Hands*, Springer Berlin Heidelberg, Berlin, Heidelberg, pp. 117–138.

[17] Bullock, I. M., Ma, R. R., and Dollar, A. M., 2013, "A Hand-Centric Classification of Human and Robot Dexterous Manipulation," IEEE Transactions on Haptics, **6**(2), pp. 129–144.

[18] Resnik, L. J., Borgia, M. L., Cancio, J. M., Delikat, J., and Ni, P., 2021, "Psychometric evaluation of the Southampton hand assessment procedure (SHAP) in a sample of upper limb prosthesis users." Journal of hand therapy : official journal of the American Society of Hand Therapists.

[19] Burger, H., Giordano, A., Mlakar, M., Albensi, C., Brezovar, D., and Franchignoni, F., 2019, "Cross-cultural adaptation and Rasch validation of the Slovene version of the Orthotics and Prosthetics Users' Survey (OPUS) Client Satisfaction with Device (CSD) in upper-limb prosthesis users," Annals of Physical and Rehabilitation Medicine, **62**(3), pp. 168–173.

[20] Waldron, K. J., Kinzel, G. L., and Agrawal, S. L., 2016, *Kinematics, Dynamics, and Design of Machinery*, 3rd ed., Wiley.

[21] Cerruti, G., Chablat, D., Gouaillier, D., and Sakka, S., 2015, "Design method for an anthropomorphic hand able to gesture and grasp," *2015 IEEE International Conference on Robotics and Automation (ICRA)*, IEEE, pp. 3660–3667.

[22] Blais, F., Picard, M., and Godin, G., 2004, "Accurate 3D acquisition of freely moving objects," *Proceedings. 2nd International Symposium on 3D Data Processing, Visualization and Transmission, 2004. 3DPVT 2004.*, pp. 422–429, doi: 10.1109/TDPVT.2004.1335269.

[23] Cerruti, G., 2016, "Design and Control of a Dexterous Anthropomorphic Robotic Hand," Ph.D. thesis, Ecole Centrale de Nantes, https://hal.archives-ouvertes.fr/tel-01396616

[24] Bennis, F. and Bhattacharjya, R. K., 2020, *Nature-Inspired Methods for Metaheuristics Optimization: Algorithms and Applications in Science and Engineering*, Vol. 16, Springer.

[25] Butin, C., Chablat, D., Aoustin, Y., and Gouaillier, D., 2022, "Design of a Two-Speed Load Adaptive Variable Transmission for Energetic Optimization of an Accessible Prosthetic Hand," Journal of Mechanisms and Robotics, **15**(1), p. 011003.

,